

# Scattering-Parameter Models and Representations for Microwave Mixers\*

Dylan F. Williams, *Fellow, IEEE*, Fabien Ndagijimana, Kate A. Remley, *Member, IEEE*, Joel Dunsmore, *Member, IEEE*, and Sean Hubert

## *Abstract*

We present straightforward models and representations for RF and image mixers, and develop simple rules for transforming electrical problems involving mixers and signals at several frequencies into equivalent single-frequency problems. We show how those models, representations, and rules can be applied to mixer characterization with vector network analyzers, and how they relate to more general descriptions based on scattering parameters currently in use.

## Paper 1967

Index terms: frequency conversion; frequency translation; image frequency; microwave; mixer; model; scattering parameters

Contact:  
Dylan Williams  
NIST 813.01  
325 Broadway  
Boulder, CO 80305  
(303)497-3138  
[dylan@boulder.nist.gov](mailto:dylan@boulder.nist.gov)

\* Publication of the National Institute of Standards and Technology, not subject to copyright.

## INTRODUCTION

We develop system-level models and representations for electrical mixers based on scattering parameters and ideal mixer blocks. The scattering parameters describe the reflections, transfer function, and degree of reciprocity of the mixers. The ideal mixer blocks describe their ideal frequency-translation behavior. Results from the experimental study of [1], some of which we present here, confirm the theory.

An electrical mixer multiplies a low-level input signal at one of its ports by a high-level local-oscillator (LO) signal at frequency  $\omega_{LO}$ . This multiplication is accomplished by using the high-level local-oscillator signal to periodically turn on and off diodes (or transistors) in the mixer, creating a time-varying conductance with the same periodicity as the LO signal. The circuit is designed so that the time-varying conductance modulates (multiplies) the low-level input signal. This temporal multiplication translates low-level signals between a (typically) low intermediate frequency (IF)  $\omega_{IF}$  at one port of the mixer and signals at an “RF” frequency  $\omega_{RF} = \omega_{LO} + \omega_{IF}$  or an “image” frequency  $\omega_{IM} = \omega_{LO} - \omega_{IF}$  at the other port of the mixer.

Electrical mixers also generate a number of other “mixing products” (additional or “spurious” frequency components) at sums and differences of the harmonics of the LO and IF, RF, and image frequencies. References [2] and [3] outline a complete circuit theory describing this behavior, which we do not address here, in terms of conversion matrices.

The conversion matrices of [2] and [3], which we discuss in greater detail in Appendix 1, express the relationships between voltages and currents, or equivalently, the forward and backward waves, at all of the frequencies generated by a mixer. While the theories of [2] and [3] are essential for mixer design, they are more complex than required for most system-

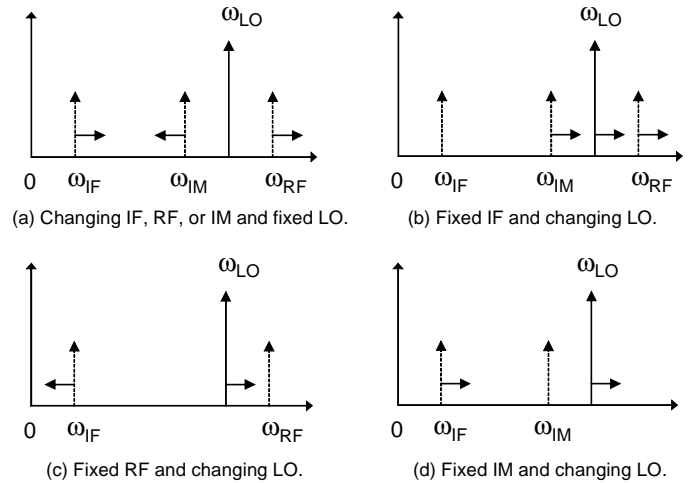


Fig. 1. The frequencies at the input and output of an electrical mixer. The horizontal arrows show how changes in the phase or frequency of an input signal change the output signal.

level design. This complexity, as well as the integration of the frequency-translating properties of the mixer into the conversion matrices themselves, obscures some important relationships and makes them difficult to use for systems design and test.

In practice, most mixers are operated as simple frequency converters in a quasilinear regime. They are configured with strong LO, small-signal inputs, and filters that allow up-conversion and down-conversion between the mixer’s IF and RF frequency, and do not create spurious signals at other frequencies. We call these standard RF mixers. We call like mixers that only allow up- and down-conversion between the IF and image frequencies “image” mixers.

Here we restrict our discussion to standard RF and image mixers satisfying these restrictions. Specifically, we ignore any spurious mixer outputs at other frequencies, and do not treat issues such as mixer nonlinearity or dependence on the level of the local oscillator signal. By restricting ourselves to a single frequency at each port, and separating the frequency-translating behavior of the mixer from its non-ideal behavior, we are able to develop models and representations that clarify system-level mixer behavior. In particular, we

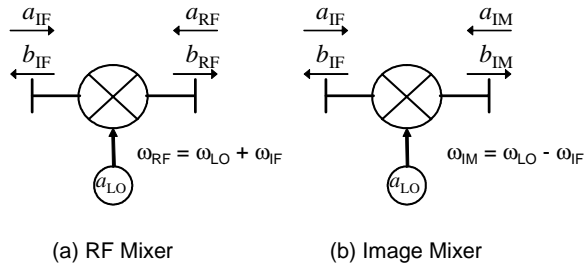


Fig. 2. Schematic and incoming and outgoing waves of an ideal mixer block.

develop a set of straightforward and intuitive rules for transforming multi-frequency mixer problems into equivalent single-frequency problems that can be solved with the simplest computer-aided-design software tools or even analytically in many cases. The rules we develop find immediate application in the characterization of mixers with vector network analyzers (VNAs). In the appendices we relate our representations to conversion matrices and large-signal scattering functions.

### BASIC MIXER OPERATION

The trigonometric identity  $\cos(A)\cos(B) = \frac{1}{2} [\cos(A+B) + \cos(A-B)]$  helps us to understand the basic operation of an electrical mixer in the time and frequency domains. For example, we can replace  $A$  in the identity with the total phase  $\omega_{LO}t + \theta_{LO}$  of a sinusoidal signal at the LO port, and  $B$  in the identity with the total phase  $\omega_{IF}t + \theta_{IF}$  of a sinusoidal signal at the IF port. This shows that the multiplication in time of the LO and IF signals results in two new frequency components at the RF (sum) frequency with total phase  $\omega_{RF}t + \theta_{RF} = (\omega_{LO} + \omega_{IF})t + (\theta_{LO} + \theta_{IF})$  and image (difference) frequency, with total phase  $\omega_{IM}t + \theta_{IM} = (\omega_{LO} - \omega_{IF})t + (\theta_{LO} - \theta_{IF})$ .

Figure 1 shows how the phases and, in like manner, the frequencies of the LO, IF, RF, and image frequencies are related. The horizontal arrows illustrate how an increase or decrease in

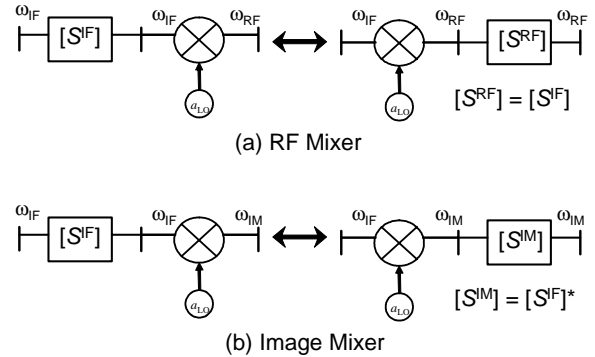


Fig. 3. Models and representations for imperfect mixers.

the phase (or frequency) of one of the input sinusoids to the mixer changes the phase (or frequency) of the mixer's output sinusoid. For example, Fig. 1a indicates that an increase in the phase of the input sinusoid at the IF will increase the phase of an output sinusoid at the RF, but *decrease* the phase of an output sinusoid at the image frequency.

We take special care to treat image mixers in our development. We will see later that the phase reversal of the IF and image signals complicates the electrical behavior of image mixers at their output ports.<sup>1</sup>

<sup>1</sup> Unlike the RF mixer, we can reverse the two ports of an ideal image mixer without changing its electrical behavior. However, to avoid confusion, we assign unique labels to the two ports of the ideal image mixer. Sticking with convention, we call one port the IF port and the other the image port.

## THE STANDARD RF MIXER

Conventional scattering parameters (i.e., the pseudo-wave scattering parameters of [4]) can be used to describe the electrical behavior of linear time-invariant electrical two-ports. The conventional scattering parameters  $S_{ij}$  relate the incident and reflected wave coefficients  $a_1$  and  $b_1$  at port 1 of the device to the incident and reflected wave coefficients  $a_2$  and  $b_2$  at port 2 of the device by

$$\begin{bmatrix} b_1 \\ b_2 \end{bmatrix} = \begin{bmatrix} S_{11} & S_{12} \\ S_{21} & S_{22} \end{bmatrix} \begin{bmatrix} a_1 \\ a_2 \end{bmatrix}. \quad (1)$$

The requirement that the frequencies on the two ports are the same is an important restriction on (1).

The ideal RF mixer of Fig. 2a acts purely as a frequency translator. Choosing the reference impedance [4] as real, the incident and reflected wave coefficients  $a_{\text{IF}}$  and  $b_{\text{IF}}$  at frequency  $\omega_{\text{IF}}$  on the IF port of the ideal RF mixer are related to the incident and reflected wave coefficients  $a_{\text{RF}}$  and  $b_{\text{RF}}$  at frequency  $\omega_{\text{RF}} = \omega_{\text{LO}} + \omega_{\text{IF}}$  on the RF port of the mixer by

$$\begin{bmatrix} b_{\text{IF}} \\ b_{\text{RF}} \end{bmatrix} = \begin{bmatrix} 0 & a_{\text{LO}}^* \\ a_{\text{LO}} & 0 \end{bmatrix} \begin{bmatrix} a_{\text{IF}} \\ a_{\text{RF}} \end{bmatrix}, \quad (2)$$

where  $a_{\text{LO}}$  is the wave coefficient of the local-oscillator signal at the ideal mixer, and a superscript \* refers to the complex conjugate, which corresponds to reversing the phase of the coefficient.

The local-oscillator power in most mixers is set at a level high enough to turn the mixing elements (the diodes or transistors) completely on and off with each cycle of the local oscillator. So, to first order, an increase or decrease in local-oscillator power does not change the mixer output. Thus, we set  $|a_{\text{LO}}| = 1$ .

Equation (2) can be understood by referring to Fig. 1. We see that increasing the phase of the

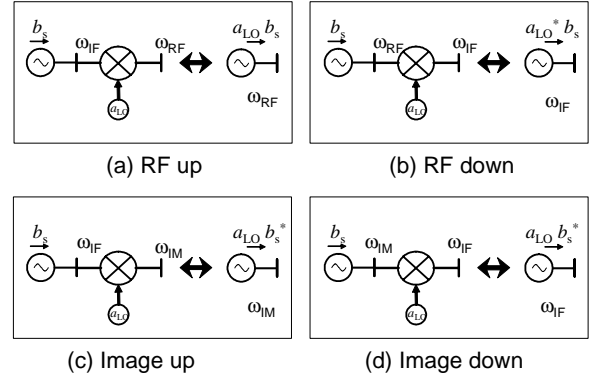


Fig. 4. Equivalent sources for RF and image mixers.

incident-wave coefficient  $a_{\text{IF}}$  at the IF port or the phase  $a_{\text{LO}}$  of the local oscillator increases the phase of the outgoing-wave coefficient  $b_{\text{RF}}$  at the RF port, as shown in Fig. 1a and 1b. Likewise, increasing the phase of  $a_{\text{RF}}$  or decreasing the phase of  $a_{\text{LO}}$  increases the phase of  $b_{\text{IF}}$ , as illustrated in Fig. 1a and 1c.

Note that, because the frequencies at the IF and RF ports of the ideal mixer are not the same, the electrical behavior of even this ideal RF mixer cannot be represented by a conventional scattering-parameter matrix. The matrix in (2) is perhaps more appropriately called a conversion matrix [5], but should not be confused with the more general conversion matrices described in [2] and [3].

Of course, no mixer is ideal: real mixers have a frequency-dependent conversion loss (or gain) and phase distortion that we will attempt to capture in our mixer representation. However, we will ignore a number of second-order nonlinear effects.

Figure 3a shows two models or representations of a nonideal RF mixer. In these mixer models, we separate the ideal frequency-translating behavior of the mixer from its nonideal behavior, which we represent in terms of standard scattering-parameters.

In the first model, all of the nonideality of the mixer caused by reflections, imperfect conversion loss, and phase distortion is described by a scattering-parameter matrix  $[S^{\text{IF}}]$

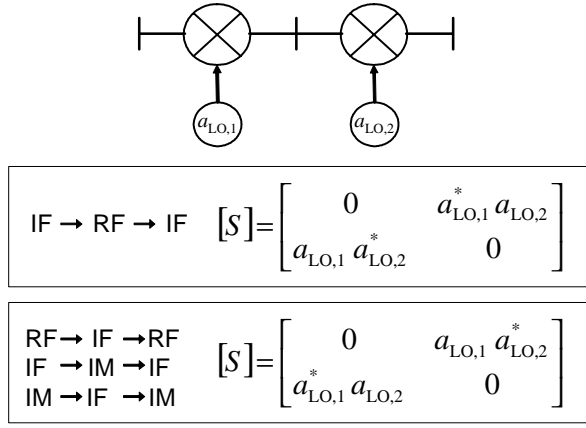


Fig. 5. Scattering parameters of two cascaded mixers with the same local-oscillator frequency. The top box shows the scattering parameters of a mixer cascade that translates signals from the IF to the RF and back to the IF frequency. The bottom box shows the scattering parameters of three other common configurations.

placed before the ideal mixer block. Here  $[S^{\text{IF}}]$  relates the wave coefficients at its two ports by (1), and those waves have the same frequency  $\omega_{\text{IF}}$ . It is the ideal mixer block to the right of  $[S^{\text{IF}}]$ , whose electrical behavior is described by equation (2), that performs the frequency translation between the IF and RF frequencies. Thus we can call  $[S^{\text{IF}}]$ , which is akin to an “error box” used to describe nonidealities in vector network analyzers, a true scattering-parameter matrix.

In the second model, the nonideality of the mixer is described by a similar scattering-parameter matrix  $[S^{\text{RF}}]$  placed after the ideal mixer block. While  $[S^{\text{RF}}]$  relates wave coefficients with frequency  $\omega_{\text{RF}}$ , rather than  $\omega_{\text{IF}}$ , the frequencies are still the same at both ports of  $[S^{\text{RF}}]$ , so we can also call  $[S^{\text{RF}}]$  a true scattering-parameter matrix.

From (1) and (2) we can readily show that, for nonideal RF mixers,

$$\begin{aligned} \begin{bmatrix} b_{\text{IF}} \\ b_{\text{RF}} \end{bmatrix} &= \begin{bmatrix} S_{11}^{\text{IF}} & a_{\text{LO}}^* S_{12}^{\text{IF}} \\ a_{\text{LO}} S_{21}^{\text{IF}} & S_{22}^{\text{IF}} \end{bmatrix} \begin{bmatrix} a_{\text{IF}} \\ a_{\text{RF}} \end{bmatrix} \\ &= \begin{bmatrix} S_{11}^{\text{RF}} & a_{\text{LO}}^* S_{12}^{\text{RF}} \\ a_{\text{LO}} S_{21}^{\text{RF}} & S_{22}^{\text{RF}} \end{bmatrix} \begin{bmatrix} a_{\text{IF}} \\ a_{\text{RF}} \end{bmatrix}. \end{aligned} \quad (3)$$

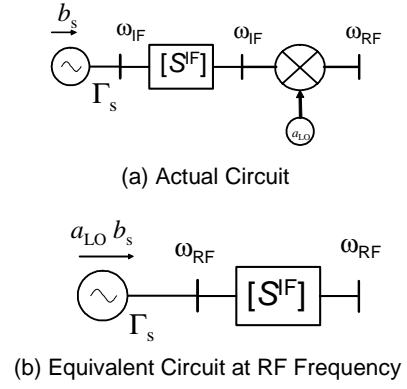


Fig. 6. Actual and equivalent circuit for a source and RF mixer.

The matrices in (3) incorporate the frequency-translating behavior of the mixers, and are similar in form of the conversion matrices discussed in [2] and [3] (see Appendix 1).

Note that the phase of  $a_{\text{LO}}$  in (3) is the phase of the LO at the ideal mixer block in the model. The phase of  $a_{\text{LO}}$  is *not* usually equal to the phase of the LO at the mixer’s local-oscillator port. This distinction is important since, while the phase of the LO at the mixer’s local-oscillator port is often measurable, the phase of  $a_{\text{LO}}$  is not.

Equation (3) shows that, while  $[S^{\text{IF}}]$  and  $[S^{\text{RF}}]$  relate incident and reflected waves at different frequencies, their elements are equal. Thus we conclude that  $[S^{\text{IF}}] = [S^{\text{RF}}]$ . This important fact is summarized graphically by the two equivalent representations shown in Fig. 3a.

We can easily show from (2) that the IF source at frequency  $\omega_{\text{IF}}$  and ideal RF mixer in Fig. 4a can be described by an equivalent RF source at frequency  $\omega_{\text{RF}}$  with source output-wave coefficient  $b_{\text{RF}} = a_{\text{LO}} b_{\text{IF}}$ . Likewise, the RF source at frequency  $\omega_{\text{RF}}$  and ideal RF down-converting mixer in Fig. 4b can be described by an equivalent IF source at frequency  $\omega_{\text{IF}}$  with source output-wave coefficient  $b_{\text{IF}} = a_{\text{LO}}^* b_{\text{RF}}$ . Finally, Fig. 5 gives the scattering parameters for two ideal “back-to-back” RF mixers.

## TRANSFORMATION TO A SINGLE-FREQUENCY PROBLEM

The relations summarized in Figs. 3-5 can be regarded as a set of rules for transforming mixer problems into equivalent single-frequency problems that can be solved with conventional procedures and formulae. The idea is to use the transformations and relations in the figures to “move” the ideal mixer blocks to the left or the right and eventually combine them either with other ideal mixer blocks or with sources.

When ideal up-converters and down-converters are combined, the result is one of the two scattering-parameter matrices shown in Fig. 5. When ideal mixer blocks are combined with sources, they simply translate the phase and frequency of the source, as illustrated in Fig. 4. In either case, the ideal mixer blocks and multiple frequencies are removed from the problem.

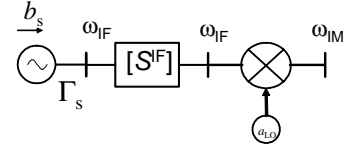
Figure 6 illustrates the application of the procedure to an example incorporating a standard RF mixer. Because of the RF mixer in the circuit, we cannot solve for the electrical behavior of the circuit of Fig. 6a with conventional scattering-parameter rules.

However, we can use the relationship summarized in Fig. 3a to interchange the position of  $[S^{IF}]$  and the ideal mixer in the circuit. Then, by splitting the source into an ideal matched source and a scattering-parameter “error box” of the form

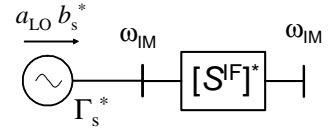
$$[S_\Gamma] = \begin{bmatrix} 0 & 0 \\ 1 & \Gamma_s \end{bmatrix}, \quad (4)$$

we can move the ideal mixer through the source reflection coefficient. Finally, we can use the relationship of Fig. 4a to combine the ideal RF mixer and source, which gives us the equivalent circuit of Fig. 6b.

We have now transformed the problem of Fig. 6a, which contains signals at both the IF



(a) Actual Circuit



(b) Equivalent Circuit at Image Frequency

Fig. 7. Actual and equivalent circuit for a source and an image mixer.

and RF frequencies, into the single-frequency problem at the RF frequency of Fig. 6b.

### THE IMAGE MIXER

The rules and transformations for standard RF mixers we discussed in the previous section were quite straight forward. Now we address the more complicated case of the image mixer.

Figure 2b shows an ideal image mixer. The incident and reflected wave coefficients  $a_{IF}$  and  $b_{IF}$  at frequency  $\omega_{IF}$  on the IF port are related to the incident and reflected wave coefficients  $a_{IM}$  and  $b_{IM}$  at the *difference* frequency  $\omega_{IM} = \omega_{LO} - \omega_{IF}$  on the image port of the mixer with

$$\begin{bmatrix} b_{IF} \\ b_{IM}^* \end{bmatrix} = \begin{bmatrix} 0 & a_{LO} \\ a_{LO}^* & 0 \end{bmatrix} \begin{bmatrix} a_{IF} \\ a_{IM}^* \end{bmatrix}. \quad (5)$$

Figure 1 also helps us to understand equation (5). For example, we see that increasing the phase of the incident-wave coefficient  $a_{IF}$  at the IF port *decreases* the phase of the outgoing-wave coefficient  $b_{IM}$  at the image port, as illustrated in Fig. 1a. This explains why the conjugate  $b_{IM}^*$  of  $b_{IM}$ , and not  $b_{IM}$ , appears in (5).

The consequences of the conjugates on  $a_{IM}$  and  $b_{IM}$  in equation (5) are profound: equation (5) cannot be rewritten in the form of equation (1) describing the way in which conventional

scattering parameters relate incident and reflected waves. This is because *increasing* the phase of an incident wave on an image mixer *decreases* the phase of the output wave at the other port. Conventional scattering parameters, on the other hand, force the phase of the output to increase when the phase of the input is increased. Thus we see that, while equation (5) is fairly straightforward, its form differs fundamentally from that of (1).

From (1) and (5) it is easy to show that, for a nonideal image mixer,

$$\begin{aligned} \begin{bmatrix} b_{\text{IF}} \\ b_{\text{IM}}^* \end{bmatrix} &= \begin{bmatrix} S_{11}^{\text{IF}} & a_{\text{LO}} S_{12}^{\text{IF}} \\ a_{\text{LO}}^* S_{21}^{\text{IF}} & S_{22}^{\text{IF}} \end{bmatrix} \begin{bmatrix} a_{\text{IF}} \\ a_{\text{IM}}^* \end{bmatrix} \\ &= \begin{bmatrix} S_{11}^{\text{IM}*} & a_{\text{LO}} S_{12}^{\text{IM}*} \\ a_{\text{LO}}^* S_{21}^{\text{IM}*} & S_{22}^{\text{IM}*} \end{bmatrix} \begin{bmatrix} a_{\text{IF}} \\ a_{\text{IM}}^* \end{bmatrix}. \end{aligned} \quad (6)$$

Thus, the two equivalent-circuit models of the image mixer in Fig. 2 are related by  $[S^{\text{IF}}] = [S^{\text{IM}*}]$ . The conjugation of the scattering parameters in  $[S^{\text{IM}}]$  is related to the fact that, like the standard RF mixer, the ideal image mixer is not time invariant, and arises from the conjugates on  $a_{\text{IM}}$  and  $b_{\text{IM}}$  in equation (5).

From the relation  $[S^{\text{IF}}] = [S^{\text{IM}*}]$ , we see that interchanging the position of an ideal image mixer and conventional scattering-parameter matrix, as illustrated in Fig. 3b, conjugates all of the elements of those scattering parameters. This is no trick we have ever seen ordinary scattering parameters perform before, and illustrates how profoundly equation (5) differs from equation (1).

Figures 4c and 4d show equivalent circuit models for sources and image mixers. The similarity of the two models is not surprising given the reversibility of the two ports of an ideal image mixer.

Finally, Fig. 5 shows the scattering parameters of two cascaded mixers with the same local-oscillator frequency. For the four configurations shown in the figure, the frequencies at the input and output of the

cascade are the same, and the cascade is described by a true scattering-parameter matrix.

## AN IMAGE-MIXER PROBLEM

We can also use the relations summarized in Figs. 3-5 to transform image-mixer problems into equivalent single-frequency problems. However, as Figs. 3-5 indicate, moving ideal image mixers through other circuits conjugates their scattering parameters.

Figure 7 illustrates the procedure for the example of Fig. 6 with an image, rather than an RF, mixer. When we use the relationship summarized in Fig. 3b to interchange the position of  $[S^{\text{IF}}]$  and the ideal image mixer in the circuit, we conjugate  $[S^{\text{IF}}]$  in the process. Likewise, when we move the ideal image mixer through the source reflection coefficient, we also conjugate  $\Gamma_s$ . Finally, using the relationship of Fig. 4c to combine the ideal image mixer and source, we obtain the equivalent circuit of Fig. 7b. We have now transformed the problem of Fig. 7a, which contains signals at both the IF and image frequencies, into the single-frequency problem at the image frequency of Fig. 7b. The equivalent circuit of Fig. 7b can be easily simulated in CAD software, or solved analytically.

## MIXER RECIPROCITY AND GROUP DELAY

Passive time-invariant circuits constructed of reciprocal materials satisfy the Lorentz reciprocity theorem, and are often called “reciprocal.” Reciprocity in this sense implies that the circuits forward and reverse transmission coefficients  $S_{21}$  and  $S_{12}$  are equal. Implicit in this statement is the fact that the input and output frequencies of the circuit are equal.

Obviously microwave mixers do not satisfy the requirements of the Lorentz reciprocity theorem, and thus would not be expected in general to be reciprocal. In fact, even an ideal RF mixer whose electrical behavior is defined

by equation (2) is not reciprocal in any strict sense, since the relationships between its input and output phases depend on the local oscillator frequency. That is, we can always choose  $a_{LO}$  in (2) so as to set the difference of the phase of  $b_{IF}/a_{RF}$  and  $b_{RF}/a_{IF}$  equal to any value we desire.

How then are we to define the reciprocity of a mixer? Perhaps the best way to define mixer reciprocity is not in terms of the mixer itself, but rather in terms of the scattering-parameters [ $S^{IF}$ ] defining the lack of ideality of the mixer. Not only do these scattering parameters relate input and output wave coefficients at the same frequency, and thus might actually be capable of being reciprocal in the conventional sense, but stating that  $S^{IF}_{21} = S^{IF}_{12}$  guarantees us that signals are distorted during up conversion and down conversion in the same way, which corresponds to what we intend to say when we claim that a mixer is reciprocal.

The difference in magnitudes of  $S^{IF}_{21}$  and  $S^{IF}_{12}$  can be determined in a straight-forward way from measurements with traceable power calibrations [5-7]. However, in most measurement situations we will be able measure the phases of the ratios  $b_{IF}/a_{RF}$  and  $b_{RF}/a_{IF}$  (and thus  $a_{LO}^* S^{IF}_{21}$  and  $a_{LO} S^{IF}_{12}$ ) and the phase of the local oscillator at the mixer port, but not the phase of  $a_{LO}$  at the ideal mixer block in the model. This is true when making measurements with oscilloscopes and three-port large-signal network analyzers [7]. In some vector network analyzer measurements [3], we cannot even measure the phase of the local oscillator at the mixer port, much less the phase of  $a_{LO}$  at the ideal mixer block in the model. Thus, in all of these situations, we are only able to measure the difference of  $S^{IF}_{21}$  and  $S^{IF}_{12}$  to within an unknown constant equal to twice the phase of the unknown local oscillator phase at the ideal mixer.

Since we are only able from measurements at the ports of a mixer to determine the difference of the phases of  $S^{IF}_{21}$  and  $S^{IF}_{12}$  to within an unknown constant, we must content ourselves with defining mixer reciprocity, or the lack of it,

in terms of the *changes* in the phases of  $S^{IF}_{21}$  and  $S^{IF}_{12}$  with frequency. The group delay  $t_g$  is a measure of the time a band-limited signal takes to pass through an electrical system, and is an ideal way to describe mixer reciprocity.

Group delay is defined by  $t_g = -d\phi/d\omega$ , where  $\phi$  is the electrical phase of the signal at the output of the network minus the electrical phase of the signal at the input of the network at the same frequency. In our context, we can define the forward and backward group delay of the mixer in terms of the phases of  $S^{IF}_{21}$  and  $S^{IF}_{12}$  measured at a fixed value of  $a_{LO}$ . Note that the group delay  $t_g$  does not depend on the absolute phase of the transfer function, which in turn depends on the absolute phase of  $a_{LO}$ , and is thus offers an ideal way of expressing the phase reciprocity of a mixer.

As we noted above, group delay is calculated from the transfer function of a system whose input and output signals are at the same frequency. The rules we developed here for translating multifrequency mixer problems into single-frequency problems are thus ideal aids in calculating the group delay of circuits containing mixers.

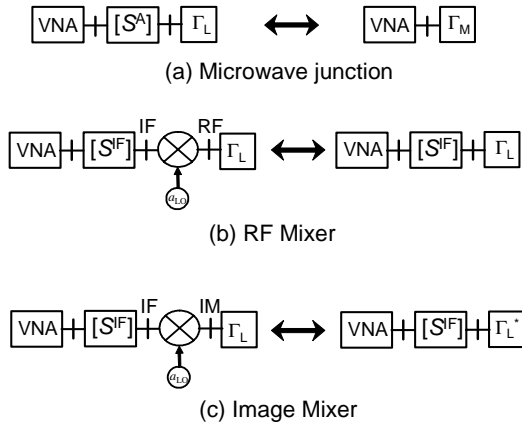


Fig. 8. Equivalent circuits for junction and mixer characterization with a VNA.

### MIXER CHARACTERIZATION WITH A VECTOR NETWORK ANALYZER

We now turn our attention to experimental results obtained from VNA measurements that illustrate the rules we have introduced for image mixers. Bauer and Penfield introduced a classic method of determining the scattering parameters of microwave junctions in Ref. [8]. They began by connecting one port of the microwave junction with unknown scattering parameters  $[S^A]$  to a calibrated VNA, as shown schematically in Fig. 8a. They then connected a load with a known reflection coefficient  $\Gamma_L$  to the other port of the junction, and used the VNA to measure the reflection coefficient of the junction and its terminating load.

The reflection coefficient  $\Gamma_M$  of the combination of the junction and its load, as measured by the VNA, is given by

$$\Gamma_M = S_{11}^A + \frac{S_{12}^A S_{21}^A \Gamma_L}{1 - S_{22}^A \Gamma_L}. \quad (7)$$

Bauer and Penfield noted that three such measurements are sufficient to determine  $S_{11}^A$ ,  $S_{22}^A$ , and the product  $S_{12}^A S_{21}^A$ , and developed a least-squares solution to make optimal use of a

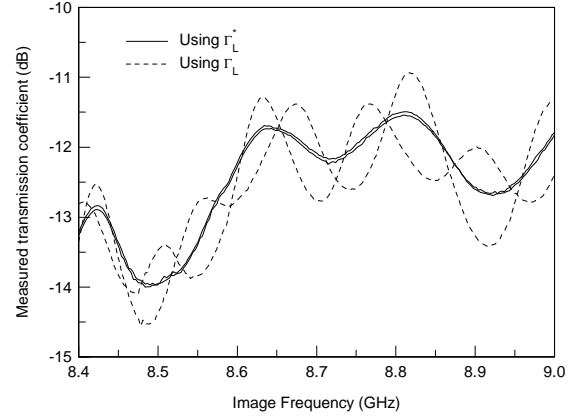


Fig. 9. Vector-network-analyzer measurement of the transmission coefficients of an image mixer and mixer/airline combination using the method of [5]. The figure shows that  $\Gamma_L$  must be replaced by  $\Gamma_L^*$  in the method of [5] to yield results consistent with the low loss and reflection coefficient of the precision airline we used in the experiment. We used a local-oscillator frequency of 9.9 GHz and the IF frequencies spanned 0.9 GHz to 1.5 GHz. Data from [1].

greater number of measurements when they were available. Finally, for passive junctions comprised entirely of reciprocal materials, Bauer and Penfield noted that  $S_{12}^A = S_{21}^A$ , allowing  $S_{12}^A$  and  $S_{21}^A$  to be determined from the measured product  $S_{12}^A S_{21}^A$ .

Dunsmore [5] adapted this idea to RF mixer characterization, using the measurement configuration sketched at the left of Fig. 8b. Dunsmore noted that (7) also applied to the RF mixer's scattering parameters  $[S^{IF}]$ . He used a variant of the classic procedure pioneered by Bauer and Penfield to solve for  $[S^{IF}]$  from a set of  $\Gamma_M$  measurements of the reflection coefficient of the mixer terminated with different loads with known reflection coefficient  $\Gamma_L$ . Dunsmore then assumed  $S_{12}^{IF} = S_{21}^{IF}$  to determine  $S_{12}^{IF}$  and  $S_{21}^{IF}$  from the measured product  $S_{12}^{IF} S_{21}^{IF}$ .<sup>2</sup>

<sup>2</sup> In the case of a microwave junction, this assumption is justified by the Lorentz reciprocity theorem and the choice of real reference impedances. Reference [2] shows that purely resistive mixers with symmetric conductance waveforms are reciprocal. However, as we discussed earlier, reciprocity is most certainly violated in diode

We can understand this procedure in the context of our mixer models and rules. First, we note that the electrical behavior of a load can be represented with a scattering-parameter matrix of the form

$$[S_\Gamma] = \begin{bmatrix} \Gamma_L & 0 \\ 0 & 0 \end{bmatrix}. \quad (8)$$

Now we can use the rule illustrated in Fig. 3a to “move” the ideal RF mixer block in Fig. 8b through the load  $\Gamma_L$ , leaving its reflection coefficient unchanged. The result is the equivalent circuit of Fig. 8b. Not only has the ideal mixer block dropped out of the equivalent circuit of Fig. 8b, but the effect of the local-oscillator phase has “cancelled” itself out completely and no longer appears in the circuit equations.

In this VNA setup, the resulting circuit in Fig. 8b is identical to that of Fig. 8a with the adapter scattering parameters  $[S^A]$  replaced by  $[S^{DF}]$ . This explains why the mixer and its local oscillator can be treated as a simple time-invariant two-port and justifies the application of (7) and the standard de-embedding methods used to characterize microwave junctions to standard RF mixers.

We can apply the same procedure to an image mixer. However, for an image mixer, we must use the rule of Fig. 3b to move the ideal mixer block through the reflection coefficient  $\Gamma_L$  of the load, conjugating  $\Gamma_L$  in the process, as shown in Fig. 8c. Thus we see that, for image mixers, we can indeed apply the classic de-embedding procedures of Bauer and Penfield and others, but must replace the reflection coefficient  $\Gamma_L$  of the load by  $\Gamma_L^*$  in the equations.

We performed three fundamental checks of this result using the measurement methods developed in [1]. In each experiment we compared the method of [5] applied to an image

---

mixers, although it may often be a reasonable approximation.

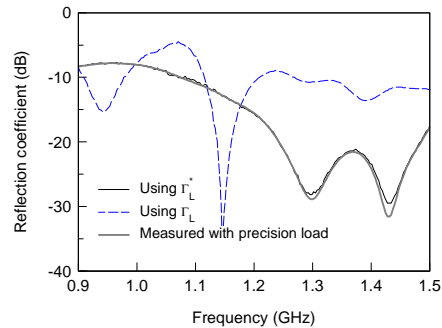


Fig. 10. Vector-network-analyzer measurement of the reflection coefficients of an image mixer and mixer/airline combination using the method of [5]. The figure shows that  $\Gamma_L$  must be replaced by  $\Gamma_L^*$  in the method of [5] to yield results consistent with a direct measurement of the reflection coefficient of the mixer terminated with a precision resistor. We used the same frequency setting in Fig. 9 and the data was measured as described in [1] and [5].

mixer using both  $\Gamma_L$  and  $\Gamma_L^*$  with an independent measurement.

#### A. Image mixer and a precision airline

We first characterized an image mixer with the method of [5]. Then we added a 5 cm precision airline to the output port of the mixer and repeated the characterization. The measured loss of the airline was about 0.05 dB and its measured reflection coefficient was less than -45 dB, so we expect the addition of the airline to modify the phase response of the image mixer while leaving its magnitude response nearly identical.

The two solid lines in Fig. 9 show the transmission coefficients obtained for the image mixer and the mixer/airline combination using  $\Gamma_L^*$  in the calculations, as derived from our theory. The measurements differ by only about 0.05 dB.

However, when we performed the calculations using  $\Gamma_L$ , rather than  $\Gamma_L^*$ , we obtained the transmission coefficients shown in dashed lines in the figure. The large discrepancy between the results we obtain using  $\Gamma_L$  in the calculations clearly illustrates the importance of

replacing  $\Gamma_L$  by  $\Gamma_L^*$  when applying the method of [5] to the characterization of image mixers.

### B. Termination in a precision load

We next terminated an image mixer in a precision load and used a conventionally calibrated VNA to measure the reflection coefficient of the mixer at its unterminated port. This reflection coefficient is, by definition, the reflection coefficient of the mixer at the unterminated port.

Figure 10 compares the reflection coefficients determined with the method of [5] using  $\Gamma_L$  and  $\Gamma_L^*$  to this more fundamental measurement of the reflection coefficient of the image mixer. The figure again shows that  $\Gamma_L$  must be conjugated when applying the method of [5] to image mixers.

### C. Power-meter-calibrated measurements

Finally, we used a power meter to directly calibrate our VNA measurements in an absolute sense at both the IF and image frequencies, and then measured the magnitudes of the forward and reverse transfer function of an image mixer directly. Figure 11 plots the ratios of the transmission coefficients determined using the method of [5] to the mean of the directly measured forward and reverse transmission coefficients. The figure shows that using  $\Gamma_L^*$  in the method of [5] to characterize an image mixer yields agrees more closely with measurements performed by our power-meter-calibrated VNA than using  $\Gamma_L$ .

## CONCLUSION

We presented models and representations for standard RF mixers and image mixers based on scattering parameters and ideal mixing blocks. These models are easily incorporated into conventional computer-aided-design tools and are suitable for systems-level analysis. We also developed a set of simple rules for analytically transforming electrical problems involving mixers and signals at several frequencies into equivalent single-frequency problems. Finally, we showed how those models, representations,

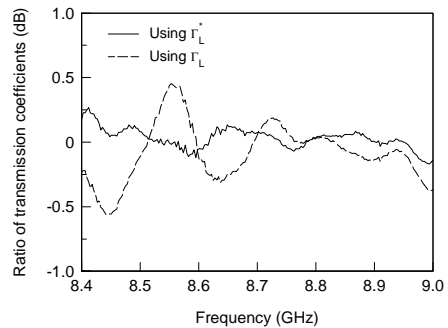


Fig. 11. Ratio of the transmission coefficients of an image mixer using the method of [5] to direct power-meter-calibrated measurements. We used the same frequency settings as for the data in Fig. 9 and the measurements were performed as described in [1] and [5].

and rules can be applied to mixer characterization with vector network analyzers. We confirm the theory with the experimental method described in [1].

The models and representations we developed are limited to mixers with a single-frequency IF port and a single-frequency RF or image port. In the appendices, we show how our representations are related to two more general representations based on scattering parameters applicable to a broader class of mixer and nonlinear problems.

## APPENDIX I

### RELATIONSHIP TO CONVERSION MATRICES

Torrey and Whitmer [2] introduced the notion of conversion matrices to describe the behavior of diode mixers in 1948. These complete conversion matrices are required for accurate mixer design, and are capable of describing spurious mixer outputs at frequencies other than the IF, RF, and image frequencies.

Maas summarized the approach of Torrey and Whitmer in [3], and defined an “S matrix,” which we will call  $S^M$ , from  $S^M \equiv (1+Y_n)^{-1}(1-Y_n)$ ,

where  $Y_n$  is the diode's conversion (admittance) matrix. Identifying Maas' port 0 with the mixer's IF port and Maas' port 1 with the mixer's RF port, we can rewrite equation (4.87) of [3] for an RF mixer as

$$\begin{bmatrix} b_{IF} \\ b_{RF} \end{bmatrix} = [S^{M,RF}] \begin{bmatrix} a_{IF} \\ a_{RF} \end{bmatrix} \equiv \begin{bmatrix} S_{00}^M & S_{01}^M \\ S_{10}^M & S_{11}^M \end{bmatrix} \begin{bmatrix} a_{IF} \\ a_{RF} \end{bmatrix}. \quad (9)$$

Comparing (3) and (9) we see that, for an RF mixer,

$$[S^{M,RF}] = \begin{bmatrix} S_{11}^{IF} & a_{LO}^* S_{12}^{IF} \\ a_{LO} S_{21}^{IF} & S_{22}^{IF} \end{bmatrix}. \quad (10)$$

Identifying Maas' port -1 with the mixer's image port, we can rewrite equation (4.88) of [3] for an image mixer as

$$\begin{bmatrix} b_{IM}^* \\ b_{IF} \end{bmatrix} = [S^{M,IM}] \begin{bmatrix} a_{IM}^* \\ a_{IF} \end{bmatrix} \equiv \begin{bmatrix} S_{-1,-1}^M & S_{-1,0}^M \\ S_{0,-1}^M & S_{0,0}^M \end{bmatrix} \begin{bmatrix} a_{IM}^* \\ a_{IF} \end{bmatrix}. \quad (11)$$

Note that Maas defined port 1 as the image port, and port 2 as the IF port in (4.88) of [3], which gives rise to the reversal of the wave coefficients in the vectors in (5) and (11). Comparing (5) and (11) we see that, for an image mixer,

$$[S^{M,IM}] = \begin{bmatrix} S_{22}^{IF} & a_{LO}^* S_{21}^{IF} \\ a_{LO} S_{12}^{IF} & S_{11}^{IF} \end{bmatrix}. \quad (12)$$

## APPENDIX II

### RELATIONSHIP TO LARGE-SIGNAL SCATTERING FUNCTIONS

Verspecht, et al. [9-11] introduced a linearization of a "large-signal scattering function" relating signals at a set harmonic

frequencies.<sup>3</sup> Part of the utility of this linearization is that its parameters can be determined by artificial neural networks from large-signal-network-analyzer measurements.

The linearization uses two complex Jacobian-like matrices  $[S_V]$  and  $[S'_V]$  to map the small-signal input vector of complex wave coefficients  $A$  into the small-signal output vector of wave coefficients  $B$  with [11]:

$$B \approx [S_V]A + [S'_V]A^*. \quad (13)$$

If we eliminate all of the elements of  $[S_V]$  and  $[S'_V]$ , except those relating the IF at the input of a mixer and the RF (or image) frequency at the output of a mixer, we can write  $A = (a_{IF}, a_{RF})^T$  and  $B = (b_{IF}, b_{RF})^T$ , where the superscript "T" indicates the transpose. Comparing (3) and (13), we see that, for an RF mixer,

$$[S_V] = \begin{bmatrix} S_{11}^{IF} & a_{LO}^* S_{12}^{IF} \\ a_{LO} S_{21}^{IF} & S_{22}^{IF} \end{bmatrix}; \quad [S'_V] = 0. \quad (14)$$

For an image mixer with  $A = (a_{IF}, a_{IM})^T$  and  $B = (b_{IF}, b_{IM})^T$  we have, from (5) and (13),

$$\begin{aligned} [S_V] &= \begin{bmatrix} S_{11}^{IF} & 0 \\ 0 & S_{22}^{IF*} \end{bmatrix} \\ [S'_V] &= \begin{bmatrix} 0 & a_{LO} S_{12}^{IF} \\ a_{LO} S_{21}^{IF*} & 0 \end{bmatrix}. \end{aligned} \quad (15)$$

### ACKNOWLEDGEMENT

The authors thank Jan Verspecht for help with Appendix II and Stephen Maas for his helpful comments.

<sup>3</sup> The linearization of [9-11] should not be confused with the "large-signal scattering parameters" of [12]. The large-signal scattering parameters of [12] relate vectors of incident and reflected large-signal wave coefficients  $\mathbf{A}$  and  $\mathbf{B}$  with a scattering matrix  $[S_J]$  via  $\mathbf{B} = [S_J] \mathbf{A}$ .

## REFERENCES

- [1] J. Dunsmore, S. Hubert, and D.F. Williams, "Vector mixer characterization for high-side LO cases," *2004 IEEE MTT-S Int. Microwave Symp.*
- [2] H.C. Torrey, C.A. Whitmer, S. Goudsmit, *Crystal Rectifiers*, New York: McGraw-Hill, 1948.
- [3] S. Maas, *Microwave Mixers*, Boston: Artech House, 1992.
- [4] R.B. Marks and D.F. Williams, "A general waveguide circuit theory," *J. Res. Nat. Instit. Standards and Technol.*, vol. 97, no. 5, pp. 533-562, Sep.-Oct. 1992.
- [5] J. Dunsmore, "Novel method for vector mixer characterization and mixer test system vector error correction," *2002 IEEE MTT-S Int. Microwave Symp. Dig.*, pp. 1833-1836, 2-7 June 2002.
- [6] A. Cidronali, K.C. Gupta, J. Jargon, K.A. Remley, D. DeGroot, and G. Manes, "Extraction of conversion matrices for P-HEMTs based on vectorial large-signal measurements," *2003 IEEE MTT-S Int. Microwave Symp. Dig.*, vol. 2, pp. 777-780, 8-13 June 2003.
- [7] W. Van Moer and Y. Rolain, "Proving the usefulness of a 3-port nonlinear vectorial network analyser through mixer measurements," *2003 IEEE MTT-S Int. Microwave Symp. Dig.*, vol. 3, pp. 1647-1650, 8-13 June 2003.
- [8] R.F. Bauer and P. Penfield, "De-embedding and unterminating," *IEEE Trans. Microwave Theory Tech.*, vol. MTT-22, no. 3, pp. 282-288, March 1974.
- [9] J. Verspecht, M. Vanden Bossche, and F. Verbeyst, "Characterizing components under large signal excitation: defining sensible 'Large signal S-parameters'?!," *49<sup>th</sup> ARFTG Conf. Dig.*, pp. 109-117, 1997.
- [10] J. Verspecht and Patrick Van Esch, "Accurately characterizing hard nonlinear behavior of microwave components with the nonlinear network measurement system: introducing 'Nonlinear Scattering Functions',"

*5<sup>th</sup> Int. Workshop on Integrated Nonlinear Microwave and Millimeterwave Circuits*, 1998.

[11] J. Verspecht, "Scattering functions for nonlinear behavioral modeling in the frequency domain," *2003 IEEE MTT-S Int. Microwave Symp. Workshop*, June 2003.

[12] J. A. Jargon, K. C. Gupta, D. Schreurs, and D. C. DeGroot, "Developing frequency-domain models for nonlinear circuits based on large-signal measurements," *Proc. XXVIIth Gen. Assembly Int. Union Radio Sci.*, CD-ROM A1.0.6, Maastricht, the Netherlands, Aug., 2002.

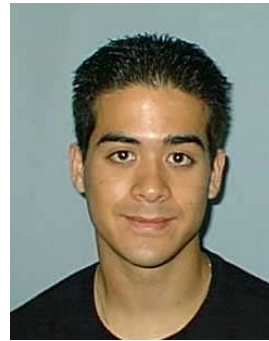


**Dylan F. Williams** (M'80-SM'90-F'02) received a Ph.D. in Electrical Engineering from the University of California, Berkeley in 1986. He joined the Electromagnetic Fields Division of the National Institute of Standards and Technology in 1989 where he develops metrology for the characterization of monolithic microwave integrated circuits and electronic interconnects. Dylan is a Fellow of the IEEE. He has published over 80 technical papers and is a Fellow of the IEEE. He is the recipient of the Department of Commerce Bronze and Silver Medals, the Electrical Engineering Laboratory's Outstanding Paper Award, two ARFTG Best Paper Awards, the ARFTG Automated Measurements Technology Award, and the IEEE Morris E. Leeds Award. Dylan is an associate editor of the IEEE Transactions on Microwave Theory and Techniques.



**Fabien Ndagijimana** is a Professor at the Université Joseph Fourier and the Institut Universitaire de Technologie (IUT) de Grenoble. He received his PhD, specializing in Microwave and optoelectronics, in December 1990, at Institut National Polytechnique de Grenoble (INPG) in France. He then joined the faculty of Electrical Engineering ENSERG as associate Professor where he teaches microwave techniques and electromagnetic modeling. His research activity in the Institut de Microélectronique d'Electromagnétisme et Photonique (IMEP) focuses on the characterization and electromagnetic modeling of microwave and high speed circuits, and their integration on silicon/SOI technologies.

applications. He has taught electrical circuit fundamentals at the local university, and presented several short courses and seminars through ARFTG, MTT, EMC, and Agilent.



**Sean Hubert** received his BS degree in computer science from the University of California at Berkeley in 2000. Since then, he has worked as a R&D software engineer for Agilent Technologies. At Agilent, Sean was a principal developer on several projects including: FTS (Filter Tuning Software), FCA (Frequency Converter Application, and the PNA (Performance Network Analyzer) firmware, and has received several patents for his work on these applications.



**Kate A. Remley** (S'92-M'99) was born in Ann Arbor, MI in December 1959. She received the B.S. degree (magna cum laude), from Oregon State University, in 1993, and the M.S. degree in 1995. She received the Ph.D. in Electrical and Computer Engineering from Oregon State University in 1999.

She worked as a Broadcast Engineer in Eugene, OR between 1983 and 1992, and was Chief Engineer of an AM/FM broadcast station from 1989-1991. She joined the Radio-Frequency Technology Division of the National Institute of Standards and Technology as an electronics engineer in 1999. Her research activities focus on development of metrology for wireless systems and characterizing the link between nonlinear circuits and system performance.



**Joel A. Dunsmore** (M'83) graduated from Oregon State University with a BSEE (1982) and an MSEE (1983). Joel has worked for Agilent Technologies (formerly Hewlett-Packard) at the Sonoma County Site. He is a senior design engineer working for the Component Test Division. He was a principle contributor to the HP 8753 and HP 8720 family of network analyzers, responsible for RF and Microwave circuit designs in these products. Recently, he has worked in the area of non-linear test including differential devices, and mixer measurements. He has received 11 patents related to this work, has published numerous articles on measurement technology, as well as consulting on measurement